Author/s:
Kalčec, N;Peranić, N;Barbir, R;Hall, CR;Smith, TA;Sani, MA;Frkanec, R;Separovic, F;Vinković Vrček, I

Title:
Spectroscopic study of L-DOPA and dopamine binding on novel gold nanoparticles towards more efficient drug-delivery system for Parkinson's disease

Date:
2022-03-05

Citation:
Kalčec, N., Peranić, N., Barbir, R., Hall, C. R., Smith, T. A., Sani, M. A., Frkanec, R., Separovic, F. & Vinković Vrček, I. (2022). Spectroscopic study of L-DOPA and dopamine binding on novel gold nanoparticles towards more efficient drug-delivery system for Parkinson's disease. Spectrochimica Acta Part A Molecular and Biomolecular Spectroscopy, 268, https://doi.org/10.1016/j.saa.2021.120707.

Persistent Link:
https://hdl.handle.net/11343/344977

Spectrochimica Acta Part A: Molecular and Biomolecular Spectroscopy 268 (2022) 120707

Contents lists available at ScienceDirect

Spectrochimica Acta Part A: Molecular and Biomolecular Spectroscopy

journal homepage: www.elsevier.com/locate/saa

Spectroscopic study of L-DOPA and dopamine binding on novel gold nanoparticles towards more efficient drug-delivery system for Parkinson's disease

Nikolina Kalčec [a], Nikolina Peranić [a], Rinea Barbir [a], Christopher R. Hall [b], Trevor A. Smith [b], Marc Antoine Sani [c], Ruža Frkanec [d], Frances Separovic [c], Ivana Vinković Vrček [a,*]

[a] Institute for Medical Research and Occupational Health, Ksaverska cesta 2, Zagreb, Croatia
[b] Australian Research Council Centre of Excellence in Exciton Science, School of Chemistry, University of Melbourne, VIC 3010 Australia
[c] School of Chemistry, Bio21 Institute, University of Melbourne, Melbourne, VIC 3010 Australia
[d] University of Zagreb, Centre for Research and Knowledge Transfer in Biotechnology, Rockefellerova 10, Zagreb, Croatia

HIGHLIGHTS

- Novel gold nanoparticles (AuNPs) were prepared using adamantyl and peptidoglycan derivatives.
- AuNPs binding affinity and loading efficiency for L-DOPA/dopamine was evaluated.
- Binding process is spontaneous and through van der Waals interactions/ hydrogen bonds or electrostatic interactions.
- A cost- and time-effective methodology for evaluating drug binding to nanomaterials is presented.

GRAPHICAL ABSTRACT

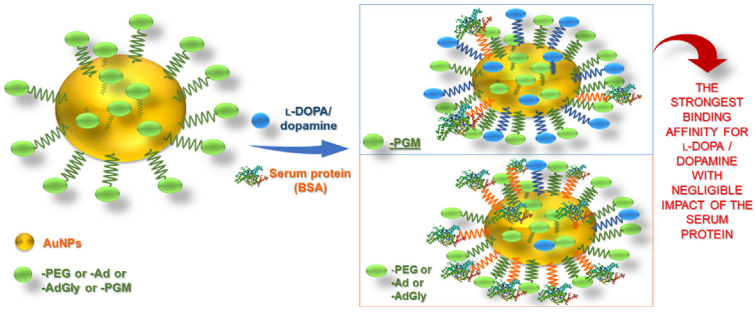

ARTICLE INFO

Article history:
Received 5 October 2021
Received in revised form 11 November 2021
Accepted 30 November 2021
Available online 6 December 2021

Keywords:
Nanodelivery system
Binding affinity
Fluorescence quenching
Drug loading efficiency
Nanoparticles

ABSTRACT

Nano-drug delivery systems may potentially overcome current challenges in the treatment of Parkinson's disease (PD) by enabling targeted delivery and more efficient blood–brain penetration ability. This study investigates novel gold nanoparticles (AuNPs) to be used as delivery systems for L-DOPA and dopamine by considering their binding capabilities in the presence and absence of a model protein, bovine serum albumin (BSA). Four different AuNPs were prepared by surface functionalization with polyethylene glycol (PEG), 1-adamantylamine (Ad), 1-adamantylglycine (AdGly), and peptidoglycan monomer (PGM). Fluorescence and UV–Vis measurements demonstrated the strongest binding affinity and L-DOPA/ dopamine loading efficiency for PGM-functionalized AuNPs with negligible impact of the serum protein presence. Thermodynamic analysis revealed a spontaneous binding process between L-DOPA or dopamine and AuNPs that predominantly occurred through van der Waals interactions/hydrogen bonds or electrostatic interactions. These results represent PGM-functionalized AuNPs as the most efficient at L-DOPA and dopamine binding with a potential to become a drug-delivery system for neurodegenerative diseases. Detailed investigation of L-DOPA/dopamine interactions with different AuNPs was described here for the first time. Moreover, this study highlights a cost- and time-effective methodology for evaluating drug binding to nanomaterials.

* Corresponding author.
E-mail address: ivinkovic@imi.hr (I. Vinković Vrček).

https://doi.org/10.1016/j.saa.2021.120707
1386-1425/

1. Introduction

L-3,4-dihydroxyphenylalanine (L-DOPA) has been the therapy of choice for Parkinson's disease (PD) since the late 1960 s due to its clinical efficacy that is still not surpassed by any other treatment [1]. PD is the second most common neurodegenerative disease characterized by the decrease in dopamine concentration in basal ganglia due to selective neurodegeneration or death of mesencephalic dopaminergic neurons in the substantia nigra pars compacta [2]. Thus, the treatment of PD patients has been mainly based on the external administration of dopamine across the blood–brain barrier (BBB) to the brain. The BBB penetration efficiency of most drugs targeting the central nervous system is limited by their physicochemical characteristics. Dopamine itself, as a water-soluble hydrophilic neurotransmitter, cannot pass the BBB contrary to its biological precursor L-DOPA [2–4]. However, the treatment with L-DOPA is associated with the development of drug tolerance and a number of side effects, including arrhythmia, gastrointestinal discomfort, extreme emotional variability, anxiety, hallucinations, and impaired social and compulsive behavior, while its therapeutic efficacy has not been proved to decrease or to mitigate the degeneration of dopaminergic neurons [5]. Consequently, the development of targeted drug delivery systems for the treatment of PD has still been encumbered with many difficulties [6]. Nanotechnology offers considerable advantages in developing nanocarrier platforms that interact with cells, tissues, and organs at a biomolecular level. Nanocarriers may overcome challenges related to targeted drug delivery, BBB crossing efficacy, and controlled drug release [6,7]. As such, nanomaterials may greatly increase pharmacological efficacy while decreasing undesired side effects of specific drugs. Among the various nanomaterials currently being explored and designed for clinical use, gold nanoparticles (AuNPs) have attracted enormous attention due to their unique optical, electrical, thermal, magnetic, chemical, and biological properties [8]. The nanosize enables dense loading of drugs on AuNP surfaces, which drastically increases therapeutic efficacy due to increased drug binding affinity to the desired target receptor [9,10]. Considering the flexibility of AuNPs for versatile surface functionalization and their ability to penetrate the BBB, they are an attractive platform for targeted drug delivery into the brain [11,12].

This study evaluated the suitability of novel AuNPs to be used as delivery systems for L-DOPA and/or dopamine. There are only a few studies on dopamine interactions with AuNPs published so far. Rout et al. [12] described the interaction of dopamine with spherical citrate-coated AuNPs, while Garabagiu [13] evaluated dopamine interaction with Au nanorods stabilized with cetyltrimethyl-ammonium bromide (CTAB). Carter *et al.* described multi-branched AuNPs functionalized with L-DOPA but did not explain their interaction [11].

Here, we aimed to improve the design of AuNPs as a drug delivery system for PD therapy by surface functionalization with 1-adamantylamine (amantadine, Ad), 1-adamantylglycine (AdGly), and peptidoglycan monomer GlcNAc-MurNAc-L-Ala-D-*iso*Gln-*meso*DAP(εNH_2)-D-Ala-D-Ala (PGM). Adamantane derivatives show beneficial properties in the context of neurodegenerative diseases, especially PD, due to their lipophilicity and BBB penetration enhancement [14–16]. Moreover, amantadine was approved by The United States Food and Drug Administration (FDA) in 1973 for use in the treatment of PD [17]. The PGM originates from the *Brevibacterium divaricatum* peptidoglycan and is an ubiquitous constituent of bacterial cell walls containing long linear glycan strands cross-linked by short peptide chains. PGM was interesting due to its biocompatibility, and versatile biological activity including antimetastatic, antitumor, and immunostimulating activity [18]. PGM is a water-soluble, non-toxic, and non-pyrogenic substance and its chemical structure is completely defined [19]. Moreover, peptide-mediated NPs have been well described as synergistic therapeutic platforms for high drug loading as both entities can carry different compounds and penetrate the BBB, while peptides can efficiently target BBB receptors [20]. Polyethylene glycol (PEG) functionalized AuNPs were included in the study for comparative purposes as PEG is a non-toxic hydrophilic polymer approved for use in drugs, for delivery to the central nervous system, and neural tissue regeneration without causing inflammation and microglia responses in the brain [21].

The ability of PEG-, Ad-, AdGly- and PGM-functionalized AuNPs as efficient carriers for L-DOPA and dopamine was evaluated for the first time by measuring their binding affinity using fluorescence and UV–Vis spectroscopy. The impact of serum albumin on the interaction of different AuNPs with L-DOPA or dopamine was additionally examined as protein corona formation on nanosurface affects the behavior of AuNPs in biological systems [22]. For this purpose, bovine serum albumin (BSA) was selected as the most abundant serum protein and due to availability of large number of scientific data on nano-bio interactions with this protein. Moreover, the presence of proteins may significantly change the pharmacokinetic and pharmacodynamic properties of drugs [23].

2. Materials and methods

2.1. Chemicals and reagents

Hydrogen tetrachloroaurate trihydrate ($HAuCl_4{\cdot}3H_2O$), L-DOPA, dopamine hydrochloride, 1-adamantylamine hydrochloride, bovine serum albumin (product number A-7906), and sodium dodecyl sulfate (SDS) were purchased from Sigma-Aldrich Chemie GmbH (Munich, Germany). Sodium borohydride ($NaBH_4$) and sodium citrate dihydrate were purchased from Alfa Aesar (Kandel, Germany), HS-EG (8)-$(CH_2)_2$-COOH (458 Da) from Iris Biotech GmbH (Germany), and sodium hydroxide (NaOH) from Kemika (Zagreb, Croatia). PGM was prepared in PLIVA, Chemical and Pharmaceutical Works (Zagreb, Croatia) by the method described in the literature [24]. AdGly was prepared in our laboratory according to previously described procedures [25]. Before use, all glassware was cleaned with 10% (v/v) HNO_3 (Merck Suprapur, Darmstadt Germany) and rinsed with ultrapure water (UPW).

2.2. Synthesis of AuNPs

Four different AuNPs were prepared following three different synthetic protocols as described in the following paragraphs.

PEG-coated AuNPs were synthesized as described by Hernandez et al. [26] by using the 14 nm spherical citrate-coated AuNPs seed (citAuNPs) obtained by the citrate reduction method described by Turkevich[27] and Frens[28] with some modifications. First, 79.5 mg of $HAuCl_4{\cdot}3H_2O$ was dissolved in 183 mL of UPW and heated under constant stirring and reflux. When the solution started to boil, 5 mL of 164 mM sodium citrate dihydrate was added. The mixture was kept boiling for 30 min until the solution color changed to wine red, whereupon citAuNPs were cooled down and kept at 4 °C in the dark. Then, a mixture containing citAuNPs (10 nM), SDS (0.028%), HS-EG-(8)-$(CH_2)_2$-COOH (52 μM), and NaOH (25 mM) was prepared in a total volume of 50 mL. The mixture was incubated for 16 h at room temperature. The excess PEG chains were removed by centrifugation at 14 000 rpm for 30 min at 4 °C and discarding the supernatant. This washing process was repeated three times, the PEG-AuNPs pellets were resuspended in UPW and kept at 4 °C in the dark.

For both Ad-AuNPs and AdGly-AuNPs, the same synthetic procedure was employed by mixing 1 mL of 10 mM $HAuCl_4{\cdot}3H_2O$ and 20 μL of 1.0 M NaOH to prepare solution **1**. Then, 0.75 mL of solution **1** and 1 mL of 0.67 mM Ad or 0.60 mM AdGly were added to 6.5 mL of UPW for preparation of Ad-AuNPs and AdGly-AuNPs, respectively. Finally, 0.5 mL aqueous solution of 15 mM $NaBH_4$ was added under constant rigorous stirring and the color turned from pale yellow to wine red, then the mixture was stirred at room temperature for 1.5 h. The Ad-AuNPs solution was centrifuged twice at 8 000 rpm for 10 min, whereas the AdGly-AuNPs solution was centrifuged twice at 10 000 rpm for 20 min. The pellets were resuspended in UPW and stored in the dark at 4 °C.

PGM-AuNPs were prepared via reduction of $HAuCl_4{\cdot}3H_2O$ by $NaBH_4$ in the presence of PGM. Briefly, 1.5 mL of 10 mM $HAuCl_4{\cdot}3H_2O$ and 1 mL of 0.12 mM PGM were mixed in 6.5 mL of UPW followed by the dropwise addition of 1 mL aqueous solution of 15 mM $NaBH_4$ under stirring. After the color turned from pale yellow to wine red, the mixture was stirred at room temperature for the next 20 min. The PGM-AuNPs were purified by centrifugation at 7 000 rpm, twice for 10 min. The pellet was resuspended in UPW and stored in the dark at 4 °C.

2.3. Physico-chemical characterization of AuNPs

In all AuNP colloidal suspensions, total Au concentrations were measured in acidified solutions (2% (v/v) HNO_3) using a graphite furnace atomic absorption spectrometer (GFAAS) (Perkin Elmer AAnalyst 600, Perkin Elmer, Shelton, USA). The Au standard solution (1000 mg/L in 5% HNO_3) purchased from Merck (Darmstadt, Germany) was used for calibration.

The hydrodynamic diameter (d_H) and zeta (ζ) potential of freshly synthesized AuNPs were obtained by dynamic (DLS) and electrophoretic light scattering (ELS) methods, respectively, using a Zetasizer Nano ZS (Malvern Instruments, Malvern, UK) equipped with a "green" laser (532 nm). The intensity of scattered light was detected at an angle of 173°. Data were processed using the ZS Xplorer Zetasizer software (Malvern Instruments, Malvern, UK). The DLS measurements also allowed the determination of the polydispersity index (PDI) [29]. DLS results were reported from the size-intensity distribution function as a mean value of six measurements and include the standard deviation (SD). The Henry equation was applied to calculate the ζ potential using the Smoluchowski approximation and the results are expressed as the mean value of three measurements ± SD.

The primary size (d) and shape of AuNPs were evaluated by transmission electron microscopy (TEM, 902A; Carl Zeiss Meditec AG, Jena, Germany). The instrument operated in a bright-field mode with an acceleration voltage of 80 kV, and the images were captured with a Canon PowerShot S50 camera. AuNPs were suspended in UPW to a final concentration of 100 mg Au/L and deposited dropwise to Formvar®-coated carbon grids. The ImageJ processing software was employed to analyse TEM images and determine d of primary particles, which were distinguished from AuNP aggregates by tracing them manually. Altogether at least 100 particles per AuNP type were included in the analysis.

2.4. Steady-state fluorescence measurements

Steady-state fluorescence measurements were performed to determine binding constants of L-DOPA and dopamine for different AuNPs in the presence and absence of BSA. An Agilent Cary Eclipse fluorescence spectrophotometer (Melbourne, Australia) and a 10-mm path length quartz cuvette were used for this purpose.

In preliminary experiments, the optimal experimental concentrations for the AuNPs and fluorophores (L-DOPA, dopamine, and BSA) were defined to avoid any inner-filter effect. When the observed fluorescence intensity was not linearly related to the AuNP concentration, an inner-filter correction[30] was introduced to the fluorescence intensities using equation Eq. (1):

$$F_{obs} = F_{corr} \times 10^{\frac{-A_{ex}\times d_{ex}}{2} + \frac{-A_{em}\times d_{em}}{2}} \quad (1)$$

where F_{obs} and F_{corr} represent the observed and corrected fluorescence intensities, respectively; A_{ex} and A_{em} are the absorbance of AuNPs at the excitation and emission wavelength, respectively; d_{ex} and d_{em} are the cuvette path length in the excitation and emission direction (in cm), respectively [31].

Quenching of L-DOPA and dopamine intrinsic fluorescence was observed after the addition of increasing concentrations of AuNPs, while the fluorophore concentration was kept constant (15 μM L-DOPA, 25 μM dopamine, and 0.5 μM BSA). The following concentrations were used when evaluating the impact of BSA on L-DOPA or dopamine binding to different AuNPs: 15 μM L-DOPA + 0.1 μM BSA and 25 μM dopamine + 0.1 μM BSA. The excitation and emission bandwidths were set at 5.0 and 10.0 nm, respectively. The fluorescence emission spectra were recorded in the range from 290 to 450 nm with the excitation wavelength set at 280 nm. Before measurement, the reaction mixture of AuNPs and fluorophores was incubated for 10 min at 288 K, 298 K, and 308 K. The emission intensities of fluorophores after exposure to various concentrations of AuNPs were used to determine the quenching mechanism between the fluorophores and AuNPs using the Stern-Volmer equation:

$$\frac{F_0}{F} = 1 + k_q\tau_0[\text{AuNPs}] = 1 + K_{SV}[\text{AuNPs}] \quad (2)$$

where F_0 and F are the fluorescence intensities in the absence and presence of AuNPs, respectively; k_q is the bimolecular quenching constant; τ_0 is the lifetime of the fluorophore in the absence of AuNPs, [AuNPs] is the molar concentration of AuNPs; and K_{SV} is the Stern-Volmer quenching constant.

As all AuNPs were spherical, their molar concentrations were calculated using the following equation:

$$[\text{AuNPs}]\left(\text{molL}^{-1}\right) = 6 \times \left(\frac{[\text{Au}]\left(\text{molL}^{-1}\right) \times M_{Au}(\text{gmol}^{-1})}{\pi \times \rho_{Au}(gnm^{-3}) \times d(nm)^3}\right) \times \left(\frac{1}{N_A(mol^{-1})}\right) \quad (3)$$

where [AuNPs] is the molar concentration of AuNPs, [Au] is the molar concentration of Au as measured by GFAAS, M_{Au} is the molecular weight of gold (196.97 g/mol), ρ_{Au} is the density of Au (1.93×10^{-20} g/nm^3), d is the primary size of AuNPs obtained from TEM images, and N_A is the Avogadro constant (6.022×10^{23} mol^{-1}) [32].

The binding constant (K) and the number of binding sites (n) for fluorophore-AuNP interactions in the absence and presence of BSA were calculated using the Hill equation[12]:

$$\log\left(\frac{F_0 - F}{F}\right) = \log K + n\log[\text{AuNPs}] \quad (4)$$

In order to reveal thermodynamic changes in the binding of L-DOPA, dopamine or BSA with novel AuNPs, the binding constants (K) at different temperatures (T) were used to calculate changes in enthalpy ($\Delta H°$) and entropy ($\Delta S°$) through the van't Hoff expression:

$$lnK = -\frac{\Delta H}{RT} + \frac{\Delta S}{R} \quad (5)$$

where R is the molar gas constant (8.31 JK^{-1}mol^{-1}).

Additionally, the Gibbs free energy change ($\Delta G°$) was calculated from the following equation:

$$\Delta G = \Delta H - T\Delta S \quad (6)$$

2.5. Time-resolved fluorescence lifetime measurements

The time-resolved fluorescence measurements were carried out using a conventional time-correlated single-photon counting (TCSPC) system. In brief, excitation pulses at 280 nm were generated by the frequency tripled output of a cavity-dumped, mode-locked Ti:sapphire laser oscillator, producing ~ 100 fs duration pulses at a repetition rate of 5.4 MHz and a wavelength of 840 nm (Coherent Mira 900 with APE PulseSwitch cavity dumper). These pulses were directed to the sample contained within a quartz cuvette with a 10 mm path length. Sample fluorescence was collected at 90°to the excitation beam and directed into an imaging spectrometer (Andor Kymera 193i spectrograph) equipped with a single-photon hybrid detector (Becker and Hickl HPM-100–07-C). Timed photon events were acquired using conventional timing electronics (Ortec model 457 time-to-amplitude converter and Ortec 9307 Picotiming constant fraction discriminator (FAST Commtec, MCA-3 multichannel analyzer)). Fluorescence dynamics were recorded at an emission wavelength of 310 nm at 298 K with and without the addition of PEG-AuNPs. The concentration of fluorophores was kept constant (15 μM L-DOPA, 25 μM dopamine, and 0.5 μM BSA), while the concentration of PEG-AuNPs ranged between 0.045 and 0.68 nM. The fluorescence decay were analysed using nonlinear least square iterative reconvolution software (FAST, Edinburgh Instruments Ltd, Livingston, UK).

2.6. Evaluations of changes in UV–Vis spectra of AuNPs

Shifts in the position of the surface plasmon resonance (SPR) signals of AuNPs after the addition of L-DOPA or dopamine were recorded using the CARY 300 UV–Vis spectrophotometer (Varian Inc., Melbourne, Australia) in the wavelength range of 400 – 800 nm. The absorption spectra were recorded 10 min after incubation of AuNPs with L-DOPA, dopamine or BSA at 298 K in a quartz cuvette with an optical path of 10 mm.

2.7. The drug loading efficiency of different AuNPs

The drug loading efficiencies (DLE) of different AuNPs were calculated by the following equation:

$$DLE(\%) = \frac{(total\ amount\ of\ drug - amount\ of\ free\ drug)}{total\ amount\ of\ drug} \quad (7)$$

Each particle type was incubated with 15 μM L-DOPA or 25 μM dopamine for 10 min at room temperature. Then, free L-DOPA or dopamine was separated from AuNPs by centrifugation using an Amicon Ultra-15 Centrifugal Filter Unit (cut-off size 10 kDa, Merck) at 5 000 × *g* at room temperature for 20 min. The amount of free L-DOPA/dopamine was determined spectrofluorimetrically using an Agilent Cary Eclipse fluorescence spectrophotometer (Melbourne, Australia).

AuNPs of three different surface areas (SAs) were tested according to the:

$$\text{total AuNPs}SA\left(nm^2/\text{L}\right) = d(nm)^2 * \pi * [\text{AuNPs}]\left(\text{molL}^{-1}\right) * N_A\left(mol^{-1}\right) \quad (8)$$

where [AuNPs] is the molar concentration of AuNPs, *d* is the primary size of AuNPs obtained from TEM images, and N_A is the Avogadro constant. The selected total *SA* was kept the same for each type of AuNPs in order to assure compatibility between results.

2.8. Statistical analysis

In order to make a better evaluation of the correlation between binding affinities and drug loading efficiencies and to clarify the impact of BSA on interactions of AuNPs and L-DOPA or dopamine, data were analysed using Pearson correlation. The whole set of data was analysed including data for L-DOPA, dopamine, and all types of AuNPs. Only *p* values less than 0.05 were considered statistically significant.

3. Results and discussion

3.1. Physicochemical characteristics of AuNPs

For the synthesis of Ad-, AdGly- and PGM-coated AuNPs, a common bottom-up approach was applied and developed for this study using $NaBH_4$ to reduce Au^{3+}. We aimed to prepare monodisperse AuNPs, with long-term stability and coated only with tested coating agents (Ad, AdGly or PGM). Thus, we developed synthetic protocol that is not based on procedures that could lead to intereferences of reagents and reaction intermediates on nanosurface caused by their adsorption. Thereofre, we omitted citrate-based protocols or protocols that employ conjugation of functionalisation agents (Ad, AdGly or PGM) on PEG-AuNPs. Optimization of the synthetic protocol was achieved by a series of experiments in which the reaction conditions (i.e., temperature, mixing time and rate, concentration of reactants) were carefully tested in order to obtain spherical and stable AuNPs with similar hydrodynamic size distribution. The particles were considered unstable if they precipitated within the period of several months after synthesis. Colloidal stability of each AuNP was additionally checked by DLS, ELS, and TEM techniques immediately, and during a three-month period, after the synthesis. The AuNPs were considered stable when *d*, d_H, and ζ potential values were not changed by>10% in the tested period. The final synthetic protocol (as described in the Materials and Methods section) yielded spherical particles with a monomodal primary size distribution close to 25 nm (Table 1 and Fig. 1).

The PEG-AuNPs, prepared by the citrate reduction method, were smaller. All AuNPs exhibited a SPR, which is dependent on NP shape and size [33]. The SPR peak of Ad-AuNPs and PGM-AuNPs was at 530 nm (Fig. 2), which indicated the same size for these two AuNP types, while AdGly-AuNPs and PEG-AuNPs were characterized by a SPR peak located at 535 nm and 520 nm, respectively. Good colloidal stability of AuNPs, as proved experimentally (see Table S2 and Figure S15 in the Supplementary Materials), was aided by electrostatic repulsion forces as evidenced by negative ζ potential values in the range between −31.5 and −18.8 mV [34].

The hydrodynamic size of all AuNPs, measured by DLS in UPW, was significantly larger than the primary one due to the presence of coating agents and a hydration shell on the nanosurface, ranging from 50.3 to 111.3 nm. Observed PDI values in the range from 0.27 to 0.40 indicated a limited size distribution of AuNPs [34–36].

3.2. Steady-state and time-resolved fluorescence measurements

Steady-state fluorescence measurements were used to determine binding affinities of L-DOPA and dopamine to the novel AuNPs developed in this study. Interaction of AuNPs with BSA was added in these experiments to provide data for subsequent evaluation of serum protein impact on drug binding affinities. PEG-AuNPs were included to allow comparison with literature data as this AuNP type has been already well studied for their interactions with BSA by other groups [37–39].

Table 1
Physico-chemical characteristics of gold nanoparticles functionalized with polyethylene glycol (PEG-AuNPs), 1-adamantylamine (Ad-AuNPs), 1-adamantylglycine (AdGly-AuNPs), and peptidoglycan monomer (PGM-AuNPs). The primary diameter (d, nm) was determined by TEM, hydrodynamic diameters (d_H, nm) in ultrapure water (UPW) and polydispersity index (PDI) were obtained by DLS, and ζ potential (mV) was measured using the ELS method. All measurements were done at 25 °C and AuNPs concentration of 100 mg Au/L.

AuNPs type	d_{TEM}/nm	d_H/nm	ζ/mV	PDI
PEG-AuNPs	15.2 ± 1.7	50.3 ± 1.1	−26.8 ± 2.9	0.39
Ad-AuNPs	23.8 ± 3.3	87.9 ± 2.0	−31.5 ± 0.4	0.27
AdGly-AuNPs	30.2 ± 4.2	111.3 ± 11.9	−31.0 ± 0.5	0.40
PGM-AuNPs	23.7 ± 2.2	86.0 ± 10.3	−18.8 ± 0.2	0.32

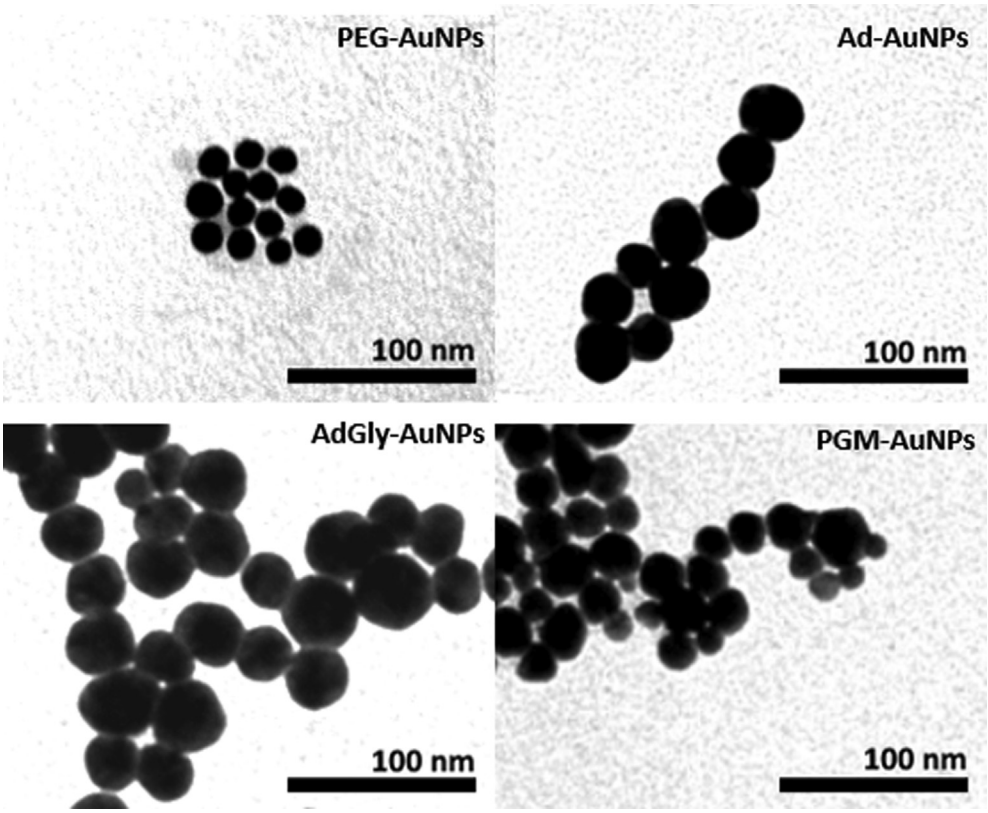

Fig. 1. Transmission electron micrographs (TEM) of PEG-AuNPs, Ad-AuNPs, AdGly-AuNPs, and PGM-AuNPs.

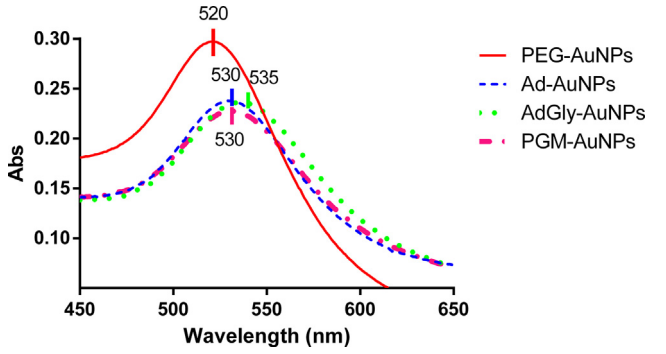

Fig. 2. UV/Vis absorption spectra of different AuNPs, dispersed in UPW at a concentration of 15 mg Au/L and 298 K.

Quenching of intrinsic fluorescence of L-DOPA, dopamine, and BSA upon exposure to various concentrations of PGM-AuNPs is shown in Fig. 3a-c. For other tested AuNPs, fluorescence quenching spectra are given in the Supporting Information (Figures S1-S3).

L-DOPA and dopamine as derivatives of phenylalanine are characterized by the maximum excitation and emission wavelengths at 280 and 317 nm, respectively [23,40]. In the case of BSA, a tryptophan residue is the dominant intrinsic fluorophore, but also other amino acids, such as tyrosine residues, contribute to its total emission quantum yield. In the absence of AuNPs, BSA exhibited a typical emission spectrum with a maximum peak at 345 nm when excited at 280 nm. The fluorescence intensity of all fluorophores was dramatically reduced with increased concentrations of each AuNP, giving a clear indication of their interaction.

The binding of L-DOPA, dopamine, and BSA to novel AuNPs was evaluated at different temperatures, as shown by Stern-Volmer plots (Fig. 4a-c and Figures S4-S6 in the Supporting Information), which typically distinguishes the dynamic from static quenching mechanism.

Static quenching occurs as a result of the formation of a non-fluorescent ground-state complex between the fluorophore and quencher, while dynamic quenching results from diffusive encounters between the fluorophore and quencher during the lifetime of the excited state [23,41,42]. In the dynamic process, the quenching rate constant increases with increasing temperature since higher temperature leads to faster diffusion and collision of the fluo-

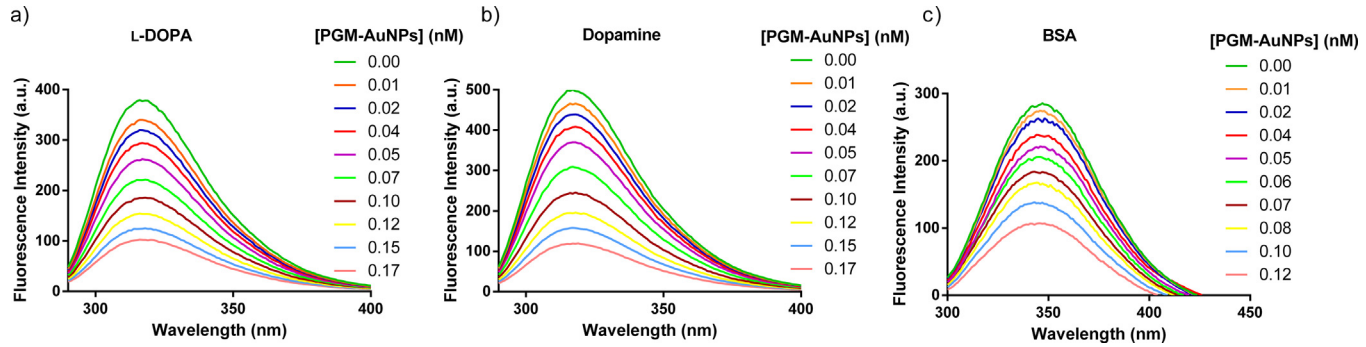

Fig. 3. Fluorescence emission spectra of a) 0.15 μM L-DOPA, b) 0.25 μM dopamine, and c) 0.5 μM bovine serum albumin (BSA) in the absence and presence of PGM-AuNPs at 298 K.

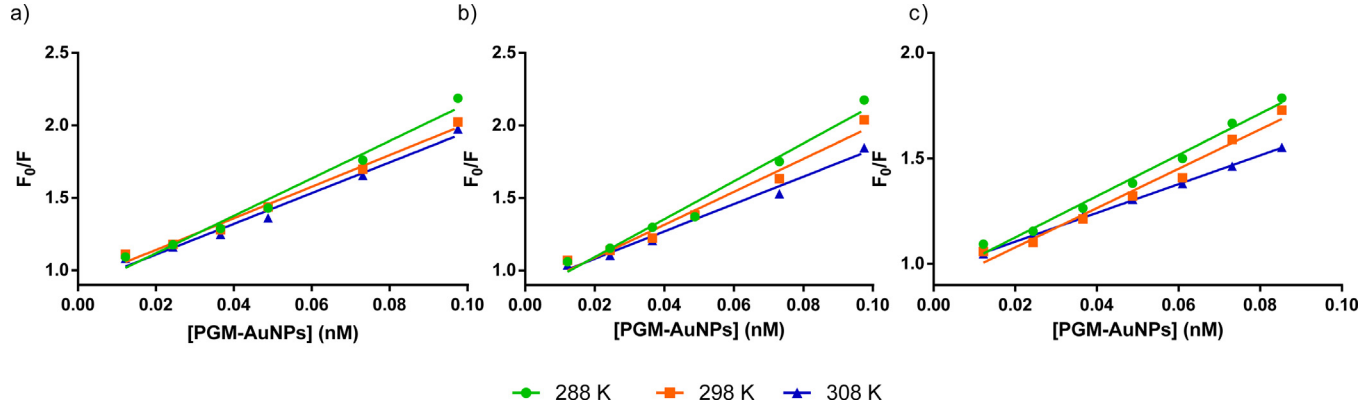

Fig. 4. The temperature-dependent Stern-Volmer plots for the fluorescence quenching of: a) L-DOPA, b) dopamine, and c) BSA by PGM-coated gold nanoparticles (AuNPs) at 288, 298, and 308 K.

rophore and the quencher. In contrast, the opposite temperature effect can be observed for the static quenching process due to the destabilization of weakly bound complexes. In some cases, both mechanisms may be involved in the interaction [23,41,42].

The Stern-Volmer plots (Fig. 4a-c and Figures S4-S6 in the Supporting Information) for binding of L-DOPA, dopamine, and BSA on PEG-, Ad-, AdGly- and PGM-coated AuNPs were well fit with a linear Stern–Volmer equation at three different temperatures (308, 298, and 288 K) suggesting that a single mechanism is involved in these interactions. Stern-Volmer quenching constants obtained by linear regression using Eq. (2) together with the bimolecular quenching constants calculated from the lifetime of the fluorophores obtained from time-resolved fluorescence measurements at 298 K, are listed in Table 2. The K_{sv} values decreased with the increasing temperature of the reaction mixture for Ad-, AdGly- and PGM-AuNPs, indicating the primary role of the static quenching process. Moreover, values of k_q were much higher than the maximum value expected of the diffusion-controlled quenching process, which should be in the order of 2.0×10^{10} M^{-1} s^{-1} [43]. Accordingly, these interactions can be described by the static quenching mechanism. In the case of PEG-AuNPs, K_{sv} values increased with temperature, which may indicate a dynamic quenching process even though the order of k_q for these interactions was higher than 10^{10} $M^{-1}s^{-1}$ [31,44].

To resolve this discrepancy, we performed time-resolved fluorescence measurements in the presence and absence of PEG-AuNPs as the most definitive method to distinguish between dynamic and static quenching by determining if the average fluorescence lifetime (τ) values of fluorophores upon interaction with quenchers will decrease or remain unchanged, respectively [42].

Fluorescence decay curves well described by single-exponential functions were obtained for L-DOPA and dopamine in the presence and absence of PEG-AuNPs, whereas the emission decay of BSA was bi-exponential, so the amplitude weighted average lifetime of BSA in the presence and absence of AuNP-PEG was calculated using:

$$< \tau >= \frac{(\alpha_1\tau_1 + \alpha_2\tau_2)}{(\alpha_1 + \alpha_{2)}} \quad (9)$$

where the$\tau_1$and τ_2 are lifetimes, and $\alpha_1$and α_2 pre-exponential factors.

The τ (<τ >) values for free L-DOPA, dopamine and BSA were 1.04 ± 0.01, 0.85 ± 0.01 and 4.78 ± 0.02 ns, respectively. Values obtained for dopamine and BSA were similar to the reported value of 0.8 ns and 5.45 ns, respectively [45,46], while the τ value for free L-DOPA is here presented for the first time. After the addition of PEG-AuNPs, there was no significant decrease in the τ values of each fluorophore, which indicated the static quenching mechanism is dominant. Moreover, plots of F_0/F vs. [PEG-AuNPs] were not consistent with plots of τ_0/τ vs. [PEG-AuNPs] for all tested fluorophores (Fig. 5) while τ_0/τ values were close to 1, which additionally confirmed a static quenching mechanism for interaction of PEG-AuNPs with selected fluorophores [42].

3.3. Binding affinities and nature of binding forces

Binding affinities (K) of L-DOPA, dopamine, and BSA to the surface of four different AuNPs, as determined using Hill plots (Fig. 6a-c and Figures S7-S9 in the Supporting Information) and Eq. (4), are given in Table 3.

Table 2
The Stern-Volmer quenching constants (K_{SV}) and bimolecular quenching constants (k_q) calculated for the interaction of PEG-, Ad-, AdGly- and PGM-coated gold nanoparticles (AuNPs) with L-DOPA, dopamine, and bovine serum albumin (BSA). Results are presented as the mean of K_{SV} and k_q values obtained from three independent measurements including standard deviations.

AuNPs type	Fluorophore	288 K $K_{sv} \times 10^9$ (M^{-1})	298 K $K_{sv} \times 10^9$ (M^{-1})	$k_q \times 10^{17}$ (M^{-1} s^{-1})	308 K $K_{sv} \times 10^9$ (M^{-1})
PEG-AuNPs	L-DOPA	0.39 ± 0.01	0.46 ± 0.01	4.44 ± 0.05	0.50 ± 0.01
Ad-AuNPs		7.75 ± 0.05	7.30 ± 0.04	70.20 ± 0.40	6.99 ± 0.08
AdGly-AuNPs		11.00 ± 0.12	10.7 ± 0.00	103.00 ± 1.00	9.97 ± 0.04
PGM-AuNPs		13.00 ± 0.60	11.30 ± 0.38	109.00 ± 3.66	10.80 ± 0.00
PEG-AuNPs	Dopamine	0.30 ± 0.00	0.36 ± 0.00	4.28 ± 0.01	0.48 ± 0.01
Ad-AuNPs		6.25 ± 0.11	6.14 ± 0.03	72.20 ± 0.34	6.02 ± 0.14
AdGly-AuNPs		9.87 ± 0.05	9.57 ± 0.02	112.00 ± 0.30	9.23 ± 0.06
PGM-AuNPs		13.20 ± 0.12	11.40 ± 0.06	134.00 ± 0.68	10.50 ± 0.14
PEG-AuNPs	BSA	0.47 ± 0.00	0.59 ± 0.01	1.24 ± 0.02	0.70 ± 0.00
Ad-AuNPs		8.58 ± 0.16	8.35 ± 0.02	17.50 ± 0.03	7.93 ± 0.52
AdGly-AuNPs		11.30 ± 0.23	9.32 ± 0.03	19.50 ± 0.07	5.81 ± 0.06
PGM-AuNPs		10.40 ± 0.07	9.17 ± 0.56	19.20 ± 1.16	7.01 ± 0.15

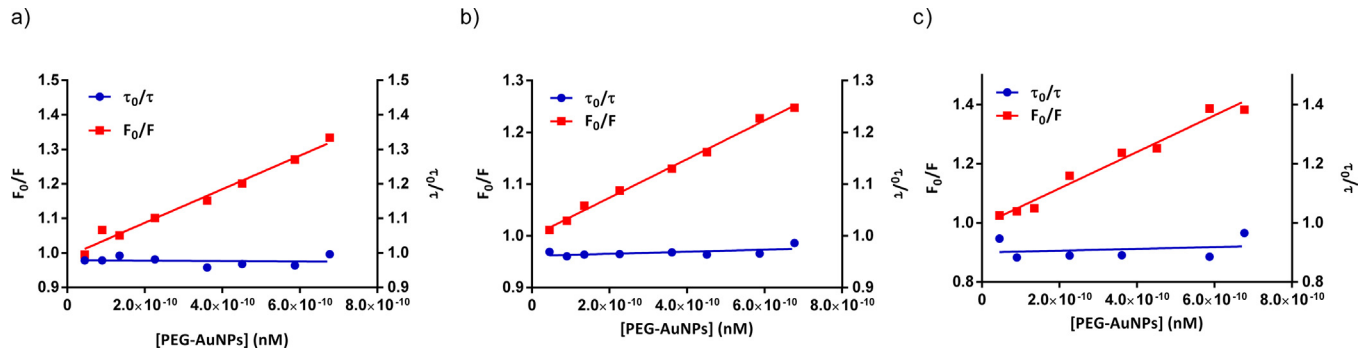

Fig. 5. Comparison of F_0/F vs. [PEG-AuNPs] and τ_0/τ vs. [PEG-AuNPs] plots obtained by time-resolved fluorescence measurements of the interaction between PEG-AuNPs and a) L-DOPA, b) dopamine, and c) bovine serum albumin (BSA) at 298 K.

The Hill coefficients (n) from Eq. (4) (listed in Table S1, Supporting Information) represent the average number of binding sites for the fluorophore-AuNP complex and are usually used to evaluate the degree of cooperativity of ligand binding. When n = 1, there is no interaction among binding sites and binding is non-cooperative, whereas n values below or above 1 indicate negative or positive cooperativity in binding, respectively [47]. A slight decrease in n values with increasing temperature was observed for all interactions (Table S1, Supporting Information). Binding of L-DOPA and dopamine to PEG-, Ad- and PGM-AuNPs was characterized by an increase in the affinity of a binding site after binding of a fluorophore to another site as indicated by $n > 1$. The AdGly-AuNPs also showed positive cooperativity at 288 K, but n was close to 1 at 298 K, whereas negative cooperativity was observed at 308 K for both L-DOPA and dopamine binding. The binding of BSA showed positive cooperativity to all tested AuNPs, which is in good agreement with earlier studies [37,48].

The strongest binding of fluorophores to the nanosurface was found for PGM-functionalized AuNPs. PGM on the surface of AuNPs may Facilitate both hydrogen bonding and electrostatic interactions with biomolecules such as amino acids and proteins, which is in favour of very strong binding interactions as evidenced by

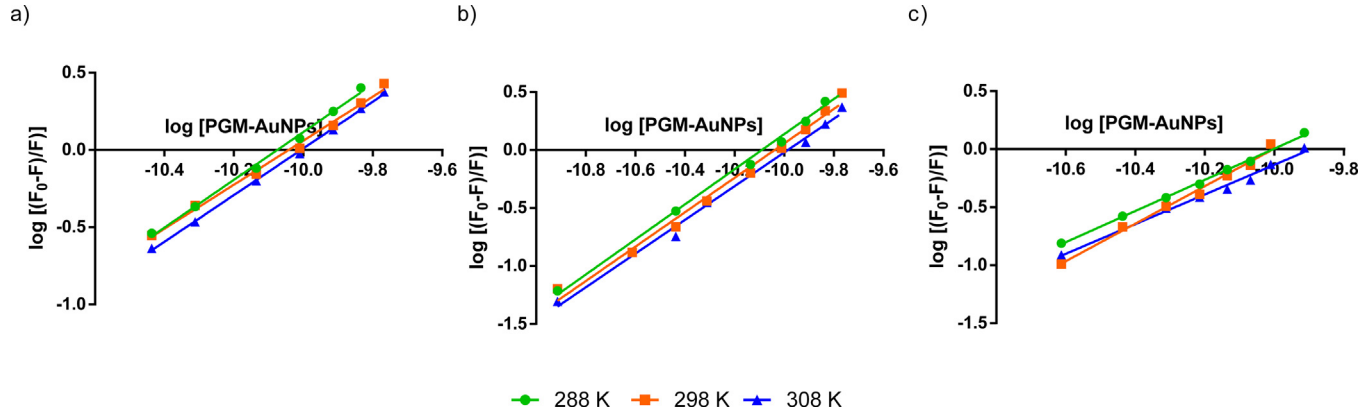

Fig. 6. The temperature-dependent Hill plots of the fluorescence quenching of a) L-DOPA, b) dopamine, and c) BS by PGM-coated gold nanoparticles (AuNPs) at 288, 298, and 308 K.

Table 3
The binding constants (K) obtained from the interaction of different gold nanoparticles (AuNPs) with L-DOPA, dopamine, and bovine serum albumin (BSA) at three different temperatures. The results are presented as the mean of K values and their corresponding standard deviation (SD) values obtained from three independent measurements.

AuNPs type	Fluorophore	$K \times 10^{10}$ (M^{-1})		
		288 K	298 K	308 K
PEG-AuNPs	L-DOPA	2.43 ± 0.17	0.96 ± 0.20	0.24 ± 0.03
Ad-AuNPs		8.40 ± 0.35	3.92 ± 0.29	1.34 ± 0.13
AdGly-AuNPs		3.51 ± 0.54	0.85 ± 0.03	0.29 ± 0.03
PGM-AuNPs		75200 ± 1040	23700 ± 4780	5760 ± 285
PEG-AuNPs	Dopamine	3.25 ± 0.38	1.07 ± 0.19	0.44 ± 0.02
Ad-AuNPs		5.56 ± 0.02	2.62 ± 0.36	0.92 ± 0.07
AdGly-AuNPs		3.06 ± 0.54	0.64 ± 0.02	0.29 ± 0.03
PGM-AuNPs		176000 ± 12000	76200 ± 3620	38200 ± 7120
PEG-AuNPs	BSA	11.80 ± 1.64	2.85 ± 0.462	0.93 ± 0.02
Ad-AuNPs		414.00 ± 38.7	186.0 ± 21.5	66.30 ± 7.50
AdGly-AuNPs		37.10 ± 0.95	10.3 ± 1.70	3.80 ± 0.33
PGM-AuNPs		2570 ± 381	476 ± 36.5	148 ± 10.4

the results shown in Table 3 [49]. Moreover, this AuNPs type is characterized by more positive ζ potential values compared to other tested AuNPs, which additionally favors interaction with negatively charged BSA and L-DOPA. Dopamine showed the strongest binding to PGM-AuNPs compared to L-DOPA and BSA, possibly due to additional electrostatic interaction of the negatively charged nanosurface with the positively charged amino group of dopamine, which was N-protonated in an acidic environment as the pH of the reaction mixture was 4.52 [50]. In the case of Ad-AuNPs, L-DOPA showed higher affinity when compared to dopamine, while their binding to PEG- and AdGly-functionalized AuNPs was quite similar and K values decreased with increasing temperature. The binding affinity of BSA to different AuNPs followed the order PGM-AuNPs > Ad-AuNPs > AdGly-AuNPs > PEG-AuNPs. Interestingly, the binding of BSA with PEG-, Ad- and AdGly-functionalized AuNPs was much stronger than the binding of L-DOPA and dopamine, while for PGM-functionalized AuNPs the opposite effect was observed. The smaller K values for the interaction of BSA and PEG-AuNPs may be influenced not only by the presence of PEG, which is one of the most used polymers for reducing or eliminating protein adsorption to surfaces but also by the particle size, i.e., PEG-AuNPs had the lowest d and d_H compared to other AuNPs. The observed K for BSA binding agrees well with earlier reports for PEG-functionalized AuNPs [37].

A decrease in K value with increasing temperature (Table 3) indicates that hydrogen bonds are the dominant forces involved in the interaction of the tested fluorophores with AuNPs since the increase in temperature destabilizes weakly bound complexes such as those based on hydrogen bonding [51,52]. Thermodynamic parameters, as calculated using van't Hoff plots (Figures S9–S11, Supporting Information) and Eq. (5) and Eq. (6) and listed in Table 4, confirmed this presumption. According to the Ross and Subramanian classification [53], the predominant interaction forces are hydrogen bonds/van der Waals interactions when ΔS and ΔH are both negative, while electrostatic interactions are predominant in the case of$\Delta S > 0$ and $\Delta H < 0$. For the interactions of L-DOPA and dopamine with PEG-, Ad- and AdGly-AuNPs, values of $\Delta S < 0$ and $\Delta H < 0$ were observed, indicating the major role of hydrogen bonding. The same was observed for the binding of L-DOPA to PGM-AuNPs. All these interactions could result from the hydrogen bonding interaction between hydroxyl groups of L-DOPA/dopamine as hydrogen donors and oxygen or nitrogen atoms on the nanosurfaces as hydrogen acceptors. In the case of hydrophilic AuNPs that are characterized by NH_2-terminated surfaces, interactions may be due to their interaction with catechol groups through hydrogen bonding or through cation–π interaction with the surface [54,55]. Only interactions of dopamine with PGM-AuNPs and that of BSA with Ad-AuNPs showed a predominantly electrostatic character (Table 4).

However, the change in enthalpy and entropy upon binding is a result of the formation and disruption of many individual interactions. Since binding of L-DOPA, dopamine, and BSA on the AuNPs surface occurred in an aqueous environment, water molecules would form hydrogen bonds with both tested fluorophores and AuNPs prior to complex formation. Water molecules must be released upon the formation of the hydrogen bonds between fluorophores and AuNPs, which increases the entropy of the system and disrupts the energetically favorable interaction, causing the enhancement in enthalpy. Thereafter, released water molecules could form bonds with other water molecules. In this way, as many new hydrogen bonds are formed as there were broken, which is an energetically favorable process ($\Delta H < 0$). Consequently, the system entropy decreased for most interactions because the total number of hydrogen bonds remained constant [49,56]. On the contrary, positive entropy changes were observed for electrostatic interactions, which reflected the release of bound water molecules from the hydrated charged molecules when they interacted [57].

A negative change in Gibbs free energy was found for all evaluated interactions (Table 4), which indicates that all binding occurred spontaneously when the system reached a state of constant pressure and temperature [56]. Moreover, an increase in temperature caused ΔH and ΔG values to become more positive due to destabilization of the weaker bonds (i.e., hydrogen and van der Waals bonds) [58].

Correlation between binding affinity and DLE is very important considering the fact that the binding affinity of NPs toward drugs should not be too low or too high. If K is too high, then an insufficient amount of drug may be released from the nanosurface in target tissues. Therefore, drug loading experiments can provide information about which nano-system would be the most suitable to deliver the drug of interest to the target [59]. Results obtained for drug loading efficiency (Fig. 7) showed dose–response that were mostly consistent with observed K values (Table 3).

In these experiments, the selected AuNPs concentrations corresponded to those applied for the fluorescence measurements, but with one additional AuNPs concentration condition corresponding to SA of 5×10^{17} nm^2/L. Consistently for observed binding affinities, the highest amount of L-DOPA and dopamine was found on the PGM-AuNPs. Moreover, the largest surface of PGM-AuNPs was loaded with > 80% of added L-DOPA and dopamine. At lower concentrations, PGM-AuNPs loaded more L-DOPA than dopamine and more than Ad- and AdGly-AuNPs. The lowest drug amount was found for PEG-AuNPs, probably due to saturation effects. Ad- and AdGly-functionalization of AuNPs showed similar results for

Table 4
The thermodynamic parameters obtained from the interaction between different gold nanoparticles (AuNPs) with L-DOPA, dopamine, and bovine serum albumin (BSA).

AuNPs type	Fluorophore	$\Delta H \times 10^4$ (kJmol^{-1})	ΔS (Jmol^{-1}K^{-1})	$\Delta G \times 10^4$ (kJmol^{-1})		
				288 K	298 K	308 K
PEG-AuNPs	L-DOPA	−8.44	−93.4	−5.75	−5.65	−5.56
Ad-AuNPs		−6.76	−25.1	−6.04	−6.01	−5.99
AdGly-AuNPs		−9.17	−117.0	−5.80	−5.69	−5.57
PGM-AuNPs		−9.46	−43.1	−8.22	−8.17	−8.13
PEG-AuNPs	Dopamine	−7.38	−55.1	−5.79	−5.73	−5.68
Ad-AuNPs		−6.63	−24.0	−5.94	−5.91	−5.89
AdGly-AuNPs		−11.0	−183.0	−5.78	−5.60	−5.41
PGM-AuNPs		−5.64	95.9	−8.40	−8.50	−8.59
PEG-AuNPs	BSA	−9.36	−114.0	−6.10	−5.98	−5.87
Ad-AuNPs		−6.74	7.93	−6.97	−6.98	−6.98
AdGly-AuNPs		−8.42	−71.1	−6.37	−6.30	−6.23
PGM-AuNPs		−10.5	−110	−7.38	−7.27	−7.16

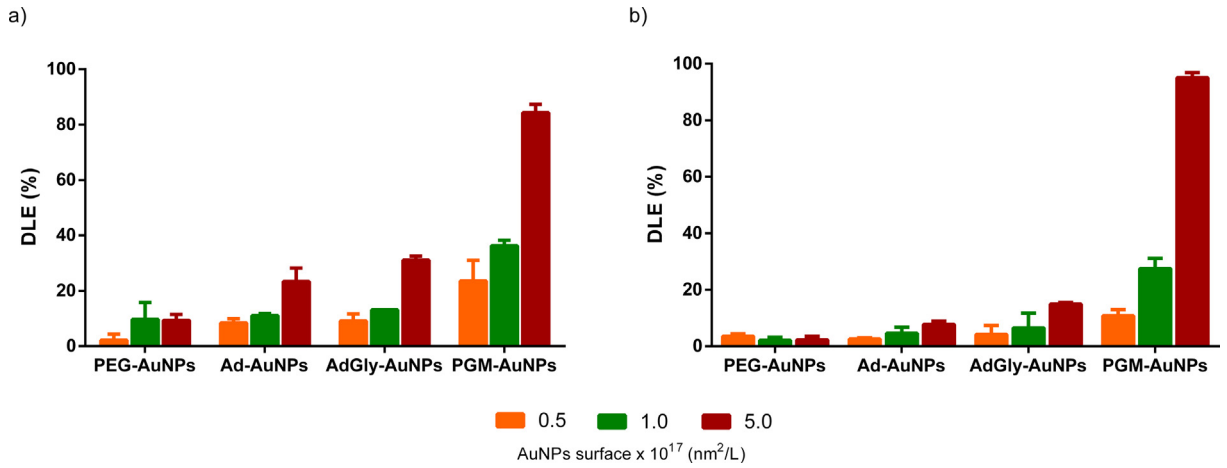

Fig. 7. Drug loading efficiency (DLE) of PEG-, Ad-, AdGly- and PGM-functionalized AuNPs for a) L-DOPA, and b) dopamine.

drug loading despite *K* values for Ad-AuNPs being much higher than for AdGly-AuNPs. Statistical analysis (Figure S12, Supporting Information) showed a positive correlation between DLE and *K* values for all tested interactions.

Upon interaction of different AuNPs with L-DOPA, dopamine or BSA, changes in size, ζ potential, and SPR peak intensity, shape, and position of the particles were also observed (Figs. 8 and 9, Figure S14 in the Supplementary Materials).

Only BSA and dopamine significantly changed the SPR peak intensity of Ad- and PGM-AuNPs possibly due to particle aggregation. As a result of plasmon coupling within AuNP aggregates, a red-shift (25–45 nm) and broadening of the plasmon band was observed after the addition of BSA, whereas a new peak at ~ 665 nm emerged for AuNPs after the addition of dopamine as a result of hydrogen-bond-mediated cross-linking between these complexes [60–64]. By comparison, changes in SPR peak intensity of PEG- and AdGly-AuNP when interacting with dopamine and BSA was almost negligible indicating more stable complexes. AuNPs displayed narrower SPR bands after the addition of L-DOPA, which reflected the stability of the L-DOPA layer around the AuNPs with a significant increase in absorbance and the most negative values of ζ potential for PGM-AuNPs, which was evidence of the formation of a highly stable complex between L-DOPA and PGM-AuNPs [65]. Moreover, there were no significant changes in hydrodynamic size and ζ potential of AuNPs after their interactions except in the case of BSA, which indicated the formation of a highly stable complex between AuNPs and drug agents [66]. It is well-known that solution pH affects BSA adsorption to nanoparticles and nanoparticle-protein association is found to be greatest at or near the isoelectric point (IEP) of the protein. As the IEP of BSA is at pH 4.5–5.0, the pH of NPs solutions used in this study was adjusted to be in this range [67]. When BSA is dissolved in an aqueous medium its hydrophilic surface can be associated with negatively charged nanosurface through electrostatic or hydrogen bonds, which is confirmed by thermodynamic analysis. However, binding processes can induce conformational changes and reorientation of protein. Hydrophobic moieties, normally internalized inside of BSA, may now be exposed and cause interactions with a hydrophobic domain of free BSA molecules and consequently lead to aggregation [68].

3.4. Impact of BSA on AuNPs interactions with L-DOPA or dopamine

The presence of proteins in biological media may significantly affect the drug binding efficiency of nanodelivery systems due to the protein corona formation around NPs [22,69]. Here, BSA was used as a representative of serum proteins and one of the most studied proteins for nano-bio interactions [23]. The effect of BSA on drug binding to different AuNPs was studied by incubating AuNPs simultaneously with the L-DOPA or dopamine and BSA solution. Results obtained for drug binding affinities in the presence of BSA (Figure S13, Supporting Information) were compared with data given in Table 3 to calculate the reduction in *K* values (Fig. 10a). Statistical analysis (Fig. 10b) revealed the highly positive correlation ($p > 0.001$) between log *K* values in the absence and log *K* values in the presence of BSA. Moreover, results indicated the same trend of reduction of log *K* values in the presence of BSA for the same type of AuNPs regardless of the drug agent tested.

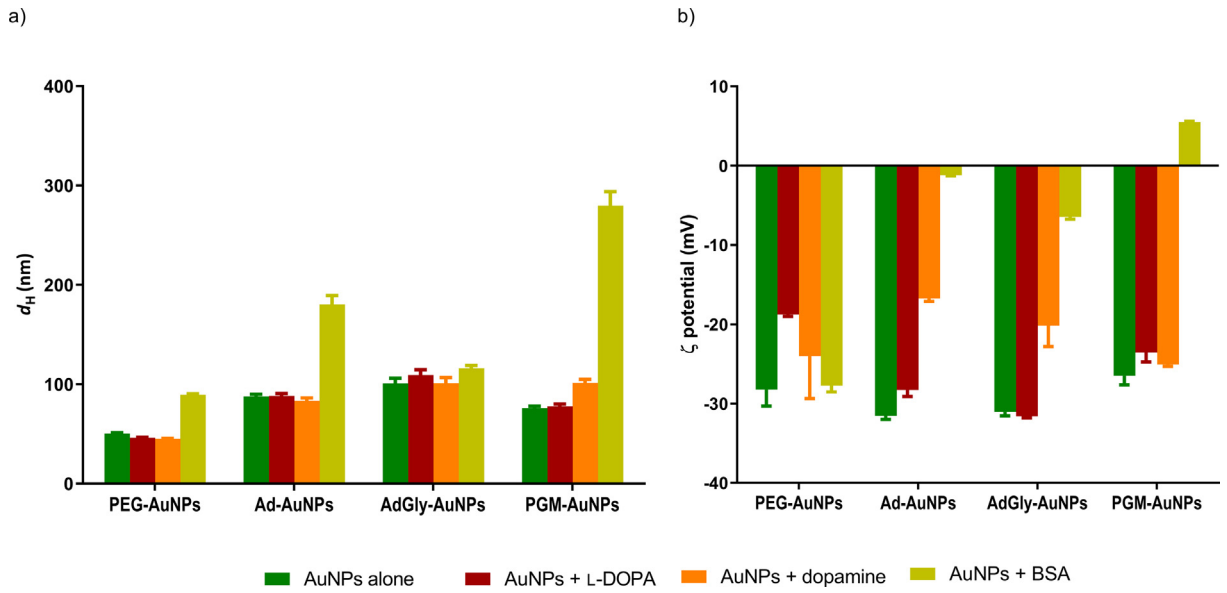

Fig. 8. Changes in a) d_H and b) ζ potential (mV) values for differently coated AuNPs before and after interaction with L-DOPA, dopamine or BSA, measured by the DLS, and ELS technique, respectively.

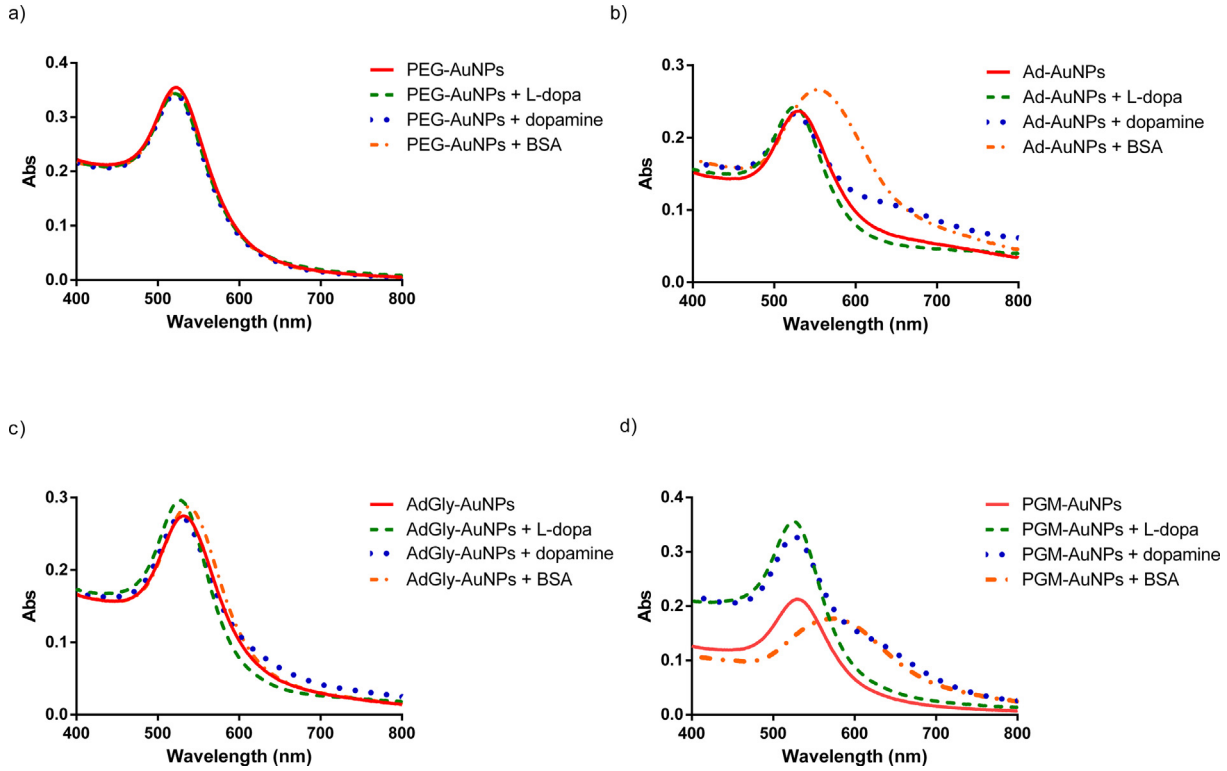

Fig. 9. Changes in SPR signals of (a) PEG-AuNPs, (b) Ad-AuNPs, (c) AdGly-AuNPs, and (d) PGM-AuNPs before and after interaction with L-DOPA, dopamine or BSA.

The addition of the BSA disturbed the equilibrium of the original binary system and its competitive binding induced a decrease in the binding affinity of L-DOPA /dopamine for all tested AuNPs (Fig. 10a). Reduction of the binding constant after the addition of BSA followed the order PEG-AuNPs ≥ AdGly-AuNPs > Ad-AuNPs > PGM-AuNPs. These results are in agreement with observed binding affinities for binary mixtures (Table 3) as L-DOPA/dopamine-AuNP complexes with smaller binding constants had a larger reduction after the addition of BSA. In addition, the reduction was greater for those AuNPs that were characterized by a greater binding affinity for BSA compared to L-DOPA or dopamine. To clarify this process, L-DOPA and dopamine showed a greater affinity for PGM-AuNPs, while BSA binding was much weaker. Consequently, L-DOPA and dopamine already bound to the nanosurface may not be easily detached and replaced by BSA [70,71] and the impact of protein on drug-loading efficiency of PGM-AuNPs was negligible. Functionalization of AuNPs with PGM probably enhanced the stability of particles in biological fluids and assure their drug loading

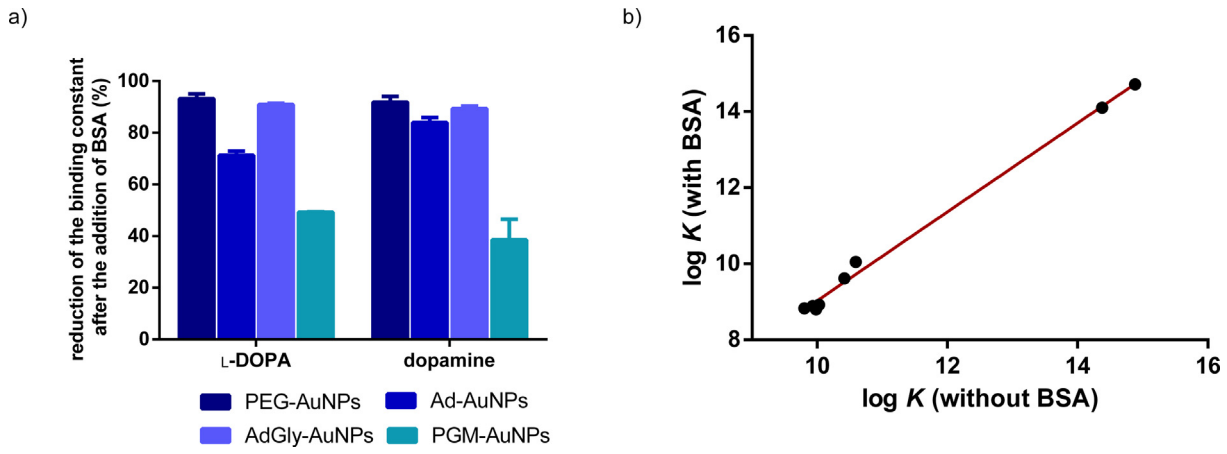

Fig. 10. a) Reduction of binding constants (in %) for interaction of L-DOPA or dopamine with PEG-, Ad-, AdGly- and PGM-functionalized AuNPs after the addition of BSA. b) Correlation of log *K* values for L-DOPA and dopamine interactions with different AuNPs in the presence and the absence of BSA.

integrity by inhibiting non-specific interactions with proteins. Thus, it can be concluded that PGM may improve the drug-loading capacity of AuNPs and their circulation lifetime in blood with a greater possibility to reach the CNS. Moreover, PGM could serve as a peptide shuttle with the ability to target the brain with minimal disruption and toxicity [20]. It is already reported that the peptidoglycans (PGN) cross the BBB through the specific pattern-recognition receptors (PRRs) of the innate immune system. There are two PRRs families on the BBB, PGN-recognition proteins (Pglyrp2) and NOD-like receptors, while the PGN transporter PepT1 is highly expressed [72]. Consequently, PGM-AuNPs may be used as a delivery system for dopamine to enable its BBB crossing and delivery to the target CNS parts. In addition, PGM-AuNPs may improve BBB penetration of L-DOPA by the large neutral amino acid transporter 1 (LAT-1). Thus, PGM-AuNPs could probably fit multiple functions, i.e., drug-delivery, BBB-penetrating, and CNS-targeting system for L-DOPA or dopamine. Thus, further evaluation of PGM-AuNPs by means of their stability, behaviour, and fate in biological media, as well as *in vitro* and *in vivo* studies are needed.

4. Conclusion

A simple synthetic strategy for the preparation of four differently functionalized AuNPs (PEG-, Ad-, AdGly- and PGM-AuNPs) was employed to prepare efficient carriers for L-DOPA and dopamine as potential drug-delivery systems. Interactions of these novel AuNPs with L-DOPA, dopamine, and BSA were investigated using versatile spectroscopic techniques. The fluorescence experiments showed fluorescence quenching of L-DOPA, dopamine, and BSA after the addition of AuNPs indicating the formation of interacting complexes. Steady-state and time-resolved measurements implied that all interactions were static in nature. The thermodynamic analysis revealed that all binding processes were spontaneous and occurred mainly due to hydrogen bonds or van der Waals interactions PGM-functionalized AuNPs showed the strongest binding affinity and drug loading efficiency towards L-DOPA and especially dopamine as a consequence of positive entropy change. This is a strong indication of the importance of electrostatic vs. van der Waals interactions in the design of nanobased drug delivery systems. Additionally, the impact of BSA on drug binding to PGM-AuNPs was almost negligible. Thus, PGM functionalization could probably fit multiple functions, i.e. efficient drug-loading, BBB-penetrating, and CNS-targeting system for L-DOPA or dopamine. However, these assumptions should be further confirmed by *in vitro* and *in vivo* investigations.

CRediT authorship contribution statement

Nikolina Kalčec: Data curation, Formal analysis, Investigation, Methodology, Visualization, Writing – original draft, Writing – review & editing. **Nikolina Peranić:** Data curation, Formal analysis, Methodology. **Rinea Barbir:** Investigation, Methodology, Formal analysis, Writing – review & editing. **Christopher R. Hall:** Data curation, Formal analysis, Methodology, Writing – review & editing. **Trevor A. Smith:** Data curation, Formal analysis, Methodology, Writing – review & editing. **Marc Antoine Sani:** Formal analysis, Writing – review & editing. **Ruža Frkanec:** Investigation, Methodology, Writing – review & editing. **Frances Separovic:** Methodology, Validation, Funding acquisition, Resources, Supervision, Writing – review & editing. **Ivana Vinković Vrček:** Conceptualization, Methodology, Funding acquisition, Project administration, Resources, Supervision, Writing – review & editing.

Declaration of Competing Interest

The authors declare that they have no known competing financial interests or personal relationships that could have appeared to influence the work reported in this paper.

Acknowledgment

This study was financially supported by the "Research Cooperability" Program of the Croatian Science Foundation funded by the European Union from the European Social Fund under the Operational Programme Efficient Human Resources 2014 – 2020 (grant HRZZ-PZS-2019-02-4323). We gratefully acknowledge support from the Australian Research Council Centre of Excellence in Exciton Science (CE170100026) and the Croatian Science Foundation (grant HRZZ-IP-2018-01-6910).

Appendix A. Supplementary material

Supplementary data to this article can be found online at https://doi.org/10.1016/j.saa.2021.120707.

References

[1] J. Xie, Z. Shen, Y. Anraku, K. Kataoka, X. Chen, Nanomaterial-based blood-brain-barrier (BBB) crossing strategies, Biomaterials 224 (2019) 119491, https://doi.org/10.1016/j.biomaterials.2019.119491.
[2] F. Haddad, M. Sawalha, Y. Khawaja, A. Najjar, R. Karaman, Dopamine and Levodopa Prodrugs for the Treatment of Parkinson's Disease, Molecules 23 (2017) 40, https://doi.org/10.3390/molecules23010040.

[3] M. Qu, Q. Lin, L. Huang, Y. Fu, L. Wang, S. He, Y. Fu, S. Yang, Z. Zhang, L. Zhang, X. Sun, Dopamine-loaded blood exosomes targeted to brain for better treatment of Parkinson's disease, J. Control. Release 287 (2018) 156–166, https://doi.org/10.1016/j.jconrel.2018.08.035.
[4] D.P. Yeggoni, R. Subramanyam, Binding studies of L-3,4-dihydroxyphenylalanine with human serum albumin, Mol. Biosyst. 10 (2014) 3101–3110, https://doi.org/10.1039/c4mb00408f.
[5] A.C. Kaushik, S. Bharadwaj, S. Kumar, D.Q. Wei, Nano-particle mediated inhibition of Parkinson's disease using computational biology approach, Sci. Rep. 8 (2018) 1–8, https://doi.org/10.1038/s41598-018-27580-1.
[6] S. Ramanathan, G. Archunan, M. Sivakumar, S.T. Selvan, A.L. Fred, S. Kumar, B. Gulyás, P. Padmanabhan, Theranostic applications of nanoparticles in neurodegenerative disorders, Int. J. Nanomedicine. 13 (2018) 5561–5576, https://doi.org/10.2147/IJN.S149022.
[7] R.R. Adhikary, P. Sandbhor, R. Banerjee, Nanotechnology platforms in Parkinson's disease, ADMET DMPK. 3 (2015) 155–181, https://doi.org/10.5599/admet.3.3.189.
[8] K. Sivaji, R.R. Kannan, Polysorbate 80 Coated Gold Nanoparticle as a Drug Carrier for Brain Targeting in Zebrafish Model, J. Clust. Sci. 30 (4) (2019) 897–906, https://doi.org/10.1007/s10876-019-01548-1.
[9] K. Hu, X. Chen, W. Chen, L. Zhang, J. Li, J. Ye, Y. Zhang, L.i. Zhang, C.-H. Li, L. Yin, Y.-Q. Guan, Neuroprotective effect of gold nanoparticles composites in Parkinson's disease model, Nanomedicine Nanotechnology, Biol. Med. 14 (4) (2018) 1123–1136, https://doi.org/10.1016/j.nano.2018.01.020.
[10] T.M. Sim, D. Tarini, S.T. Dheen, B.H. Bay, D.K. Srinivasan, Nanoparticle-based technology approaches to the management of neurological disorders, Int. J. Mol. Sci. 21 (2020) 1–32, https://doi.org/10.3390/ijms21176070.
[11] D.A. Gonzalez-Carter, Z.Y. Ong, C.M. McGilvery, I.E. Dunlop, D.T. Dexter, A.E. Porter, L-DOPA functionalized, multi-branched gold nanoparticles as brain-targeted nano-vehicles, Nanomedicine Nanotechnology, Biol. Med. 15 (1) (2019) 1–11, https://doi.org/10.1016/j.nano.2018.08.011.
[12] J. Rout, B.C. Swain, P.P. Mishra, U. Tripathy, Spectroscopic insight into the interaction of dopamine with spherical gold nanoparticles, J. Photochem. Photobiol. B Biol. 203 (2020) 111770, https://doi.org/10.1016/j.jphotobiol.2019.111770.
[13] S. Garabagiu, The quenching effect of dopamine fluorescence in the presence of gold nanorods, AIP Conf. Proc. 1565 (2013) 215–218, https://doi.org/10.1063/1.4833730.
[14] L. Wanka, K. Iqbal, P.R. Schreiner, The lipophilic bullet hits the targets: Medicinal chemistry of adamantane derivatives, Chem. Rev. 113 (5) (2013) 3516–3604, https://doi.org/10.1021/cr100264t.
[15] A. Štimac, M. Šekutor, K. Mlinarić-Majerski, L. Frkanec, R. Frkanec, Adamantane in Drug Delivery Systems and Surface Recognition, Molecules 22 (2017) 297, https://doi.org/10.3390/molecules22020297.
[16] R. Frkanec, V. Noethig-Laslo, B. Vranešić, K. Mirosavljević, J. Tomašić, A spin labelling study of immunomodulating peptidoglycan monomer and adamantyltripeptides entrapped into liposomes, Biochim. Biophys. Acta - Biomembr. 1611 (1-2) (2003) 187–196, https://doi.org/10.1016/S0005-2736(03)00054-3.
[17] G.E. Aranda-Abreu, J.D. Aranda-Martínez, R. Araújo, M.E. Hernández-Aguilar, D. Herrera-Covarrubias, F. Rojas-Durán, Observational study of people infected with SARS-Cov-2, treated with amantadine, Pharmacol. Reports. 72 (6) (2020) 1538–1541, https://doi.org/10.1007/s43440-020-00168-1.
[18] I. Tomašić, J., Hršak, Peptidoglycan monomer originating from Brevibacterium divaricatum - its metabolism and biological activities in the host., in: U. Schrinner, E., Richmond, M.H., Seibert, G., Schwartz (Ed.), Surf. Struct. Microorg. Their Interact. with Mamm. Host, VCH, Weinheim, 1987: pp. 113–121.
[19] H. Matter, L. Szilágyi, P. Forgó, Ž. Marinić, B. Klaić, Structure and dynamics of a peptidoglycan monomer in aqueous solution using NMR spectroscopy and simulated annealing calculations, J. Am. Chem. Soc. 119 (9) (1997) 2212–2223, https://doi.org/10.1021/ja962776z.
[20] M. McCully, M. Sanchez-Navarro, M. Teixido, E. Giralt, Peptide Mediated Brain Delivery of Nano- and Submicroparticles: A Synergistic Approach, Curr. Pharm. Des. 24 (13) (2018) 1366–1376, https://doi.org/10.2174/1381612824666171201115126.
[21] Q. Yan, X. Chen, H. Gong, P. Qiu, X. Xiao, S. Dang, A. Hong, Y. Ma, Delivery of a TNF-a–derived peptide by nanoparticles enhances its antitumor activity by inducing cell-cycle arrest and caspase-dependent apoptosis, FASEB J. 32 (2018) 6948–6964, https://doi.org/10.1096/fj.201800377R.
[22] A.O. Luby, E.K. Breitner, K.K. Comfort, Preliminary protein corona formation stabilizes gold nanoparticles and improves deposition efficiency, Appl. Nanosci. 6 (6) (2016) 827–836, https://doi.org/10.1007/s13204-015-0501-z.
[23] K. Phopin, W. Ruankham, S. Prachayasittikul, V. Prachayasittikul, T. Tantimongcolwat, Insight into the Molecular Interaction of Cloxyquin (5-chloro-8-hydroxyquinoline) with Bovine Serum Albumin: Biophysical Analysis and Computational Simulation, Int. J. Mol. Sci. 21 (2019) 249, https://doi.org/10.3390/ijms21010249.
[24] D. Keglević, B. Ladešić, J. Tomašić, Z. Valinger, R. Naumski, Isolation procedure and properties of monomer unit from lysozyme digest of peptidoglycan complex excreted into the medium by penicillin-treated Brevibacterium divaricatum mutant, Biochim. Biophys. Acta - Gen. Subj. 585 (2) (1979) 273–281, https://doi.org/10.1016/0304-4165(79)90027-8.
[25] B. Gašpert, S. Hromadko, B. Vranešić, Synthesis of a-Amino-1-Adamantylacetic and a-Amino- -2-Adamantylacetic Acid*, Croat. Chem. Acta. 48 (1976) 169–178.
[26] Y. Hernandez, R. González-Pastor, C. Belmar-Lopez, G. Mendoza, J.M. de la Fuente, P. Martin-Duque, Gold nanoparticle coatings as efficient adenovirus carriers to non-infectable stem cells, RSC Adv. 9 (3) (2019) 1327–1334, https://doi.org/10.1039/C8RA09088B.
[27] J. Turkevich, P.C. Stevenson, J. Hillier, A study of the nucleation and growth processes in the synthesis of colloidal gold, Discuss. Faraday Soc. 11 (1951) 55–75, https://doi.org/10.1039/DF9511100055.
[28] G. FRENS, Controlled Nucleation for the Regulation of the Particle Size in Monodisperse Gold Suspensions, Nat. Phys. Sci. 241 (105) (1973) 20–22, https://doi.org/10.1038/physci241020a0.
[29] B.A. Cornell, G.C. Fletcher, J. Middlehurst, F. Separovic, The lower limit to the size of small sonicated phospholipid vesicles, BBA - Biomembr. 690 (1) (1982) 15–19, https://doi.org/10.1016/0005-2736(82)90233-4.
[30] S.K. Panigrahi, A.K. Mishra, Study on the dependence of fluorescence intensity on optical density of solutions: the use of fluorescence observation field for inner filter effect corrections, Photochem. Photobiol. Sci. 18 (2) (2019) 583–591, https://doi.org/10.1039/C8PP00498F.
[31] C. Hao, G. Xu, Y. Feng, L. Lu, W. Sun, R. Sun, Fluorescence quenching study on the interaction of ferroferric oxide nanoparticles with bovine serum albumin, Spectrochim. Acta - Part A Mol. Biomol. Spectrosc. 184 (2017) 191–197, https://doi.org/10.1016/j.saa.2017.05.004.
[32] A. Zuber, M. Purdey, E. Schartner, C. Forbes, B. Van Der Hoek, D. Giles, A. Abell, T. Monro, H. Ebendorff-Heidepriem, Detection of gold nanoparticles with different sizes using absorption and fluorescence based method, Sensors Actuat. B Chem. 227 (2016) 117–127, https://doi.org/10.1016/j.snb.2015.12.044.
[33] W. Haiss, N.T.K. Thanh, J. Aveyard, D.G. Fernig, Determination of Size and Concentration of Gold Nanoparticles from UV−Vis Spectra, Anal. Chem. 79 (11) (2007) 4215–4221, https://doi.org/10.1021/ac070208410.1021/ac0702084.s001.
[34] E. Joseph, G. Singhvi, Multifunctional nanocrystals for cancer therapy: a potential nanocarrier, in: A.M. Grumezescu (Ed.), Nanomater. Drug Deliv. Ther., Elsevier, 2019: pp. 91–116. https://doi.org/10.1016/B978-0-12-816505-8.00007-2.
[35] G.S. El Hebeish A, Utilization of Crosslinked Starch Nanoparticles as a Carrier for Indomethacin and Acyclovir Drugs, J. Nanomed. Nanotechnol. 06 (2015) 1–8. https://doi.org/10.4172/2157-7439.1000254.
[36] P. Eaton, P. Quaresma, C. Soares, C. Neves, M.P. de Almeida, E. Pereira, P. West, A direct comparison of experimental methods to measure dimensions of synthetic nanoparticles, Ultramicroscopy 182 (2017) 179–190, https://doi.org/10.1016/j.ultramic.2017.07.001.
[37] Stefano P. Boulos, Tyler A. Davis, Jie An Yang, Samuel E. Lohse, Alaaldin M. Alkilany, Lisa A. Holland, Catherine J. Murphy, Nanoparticle-protein interactions: A thermodynamic and kinetic study of the adsorption of bovine serum albumin to gold nanoparticle surfaces, Langmuir 29 (48) (2013) 14984–14996, https://doi.org/10.1021/la402920f.
[38] R. Nicoară, M. Ilieș, A. Uifălean, C.A. Iuga, F. Loghin, Quantification of the PEGylated Gold Nanoparticles Protein Corona. Influence on Nanoparticle Size and Surface Chemistry, Appl. Sci. 9 (2019) 4789, https://doi.org/10.3390/app9224789.
[39] Sergio Dominguez-Medina, Steven McDonough, Pattanawit Swanglap, Christy F. Landes, Stephan Link, In situ measurement of bovine serum albumin interaction with gold nanospheres, Langmuir 28 (24) (2012) 9131–9139, https://doi.org/10.1021/la3005213.
[40] H.Y. Wang, Y. Sun, B. Tang, Study on fluorescence property of dopamine and determination of dopamine by fluorimetry, Talanta 57 (2002) 899–907, https://doi.org/10.1016/S0039-9140(02)00123-6.
[41] Arunkumar T. Buddanavar, Sharanappa T. Nandibewoor, Multi-spectroscopic characterization of bovine serum albumin upon interaction with atomoxetine, J. Pharm. Anal. 7 (3) (2017) 148–155, https://doi.org/10.1016/j.jpha.2016.10.001.
[42] Joseph R. Lakowicz (Ed.), Principles of Fluorescence Spectroscopy, Springer US, Boston, MA, 2006.
[43] Jianli Liu, Yonglin He, Dan Liu, Yin He, Zhipeng Tang, Hong Lou, Yapeng Huo, Xiangyu Cao, Characterizing the binding interaction of astilbin with bovine serum albumin: A spectroscopic study in combination with molecular docking technology, RSC Adv. 8 (13) (2018) 7280–7286, https://doi.org/10.1039/C7RA13272G.
[44] M.B. Shahsavani, S. Ahmadi, M.D. Aseman, S.M. Nabavizadeh, M.M. Alavianmehr, R. Yousefi, Comparative study on the interaction of two binuclear Pt (II) complexes with human serum albumin: Spectroscopic and docking simulation assessments, J. Photochem. Photobiol. B Biol. 164 (2016) 323–334, https://doi.org/10.1016/j.jphotobiol.2016.09.035.
[45] M. Mabuchi, J. Shimada, K. Okamoto, Y. Kawakami, S. Fujita, K. Matsushige, Time-Resolved Fluorescence Spectroscopy of Dopamine in the Single Cells, Proc. SPIE 4252 (2001) 140–148, https://doi.org/10.1117/12.426738.
[46] Suma K. Pawar, Seetharamappa Jaldappagari, Interaction of repaglinide with bovine serum albumin: Spectroscopic and molecular docking approaches, J. Pharm. Anal. 9 (4) (2019) 274–283, https://doi.org/10.1016/j.jpha.2019.03.007.
[47] D.I. Cattoni, Osvaldo Chara, Sergio B. Kaufman, F. Luis González Flecha, Elena Papaleo, Cooperativity in binding processes: New insights from phenomenological modeling, PLoS One. 10 (12) (2015) e0146043, https://doi.org/10.1371/journal.pone.0146043.
[48] Rinea Barbir, Barbara Pem, Nikolina Kalčec, Stephan Kastner, Katia Podlesnaia, Andrea Csáki, Wolfgang Fritzsche, Ivana Vinković Vrček, Vinković Vrček,

Application of Localized Surface Plasmon Resonance Spectroscopy to Investigate a Nano-Bio Interface, Langmuir 37 (5) (2021) 1991–2000, https://doi.org/10.1021/acs.langmuir.0c03569.
[49] G. Klebe, Protein-Ligand Interactions as the Basis for Drug Action, in: A.E. Scapin G., Patel D. (Ed.), Multifaceted Roles Crystallogr. Mod. Drug Discov. NATO Sci. Peace Secur. Ser. A Chem. Biol., Springer, Dordrecht, 2015: pp. 83–92. https://doi.org/10.1007/978-94-017-9719-1_7.
[50] Y. Bu, S.W. Lee, The characteristic Agcore Aushell nanoparticles as sers substrates in detecting dopamine molecules at various pH ranges, Int. J. Nanomed. 10 (2015) 47–54, https://doi.org/10.2147/IJN.S88308.
[51] S. Özdemir, E. Biçer, Temperature effect on binding affinity and stoichiometry between some steroids and human serum albumin, J. Chil. Chem. Soc. 61 (2016) 2809–2815, https://doi.org/10.4067/S0717-97072016000100013.
[52] Tahmid I. Mizan, Phillip E. Savage, Robert M. Ziff, Temperature Dependence of Hydrogen Bonding in Supercritical Water, J. Phys. Chem. 100 (1) (1996) 403–408, https://doi.org/10.1021/jp951561t.
[53] Philip D. Ross, S. Subramanian, Thermodynamics of Protein Association Reactions: Forces Contributing to Stability, Biochemistry 20 (11) (1981) 3096–3102, https://doi.org/10.1021/bi00514a017.
[54] Wei Zhang, Hui Yang, Fanghui Liu, Ting Chen, Guangxin Hu, Donghong Guo, Qingfeng Hou, Xu Wu, Yu Su, Jinben Wang, Molecular interactions between DOPA and surfaces with different functional groups: A chemical force microscopy study, RSC Adv. 7 (52) (2017) 32518–32527, https://doi.org/10.1039/C7RA04228K.
[55] Hao-Cheng Yang, Ruben Z. Waldman, Ming-Bang Wu, Jingwei Hou, Lin Chen, Seth B. Darling, Zhi-Kang Xu, Dopamine: Just the Right Medicine for Membranes, Adv. Funct. Mater. 28 (8) (2018) 1705327, https://doi.org/10.1002/adfm.v28.810.1002/adfm.201705327.
[56] X. Du, Y. Li, Y.-L. Xia, S.-M. Ai, J. Liang, P. Sang, X.-L. Ji, S.-Q. Liu, Insights into Protein-Ligand Interactions: Mechanisms, Models, and Methods, Int. J. Mol. Sci. 17 (2016) 144, https://doi.org/10.3390/ijms17020144.
[57] G. Nancollas, The Thermodynamics of Formation of Metal Complexes and Ion-Pairs in Solution, Croat. Chem. Acta 42 (1970) 299–310.
[58] P.D. Ross, M.V. Rekharsky, Thermodynamics of hydrogen bond and hydrophobic interactions in cyclodextrin complexes, Biophys. J. 71 (4) (1996) 2144–2154, https://doi.org/10.1016/S0006-3495(96)79415-8.
[59] M. Prabaharan, Characterization of tissue scaffolds drug release profiles, in: P. Tomlins (Ed.), Characterisation Des. Tissue Scaffolds, seventh ed., Elsevier, 2016, pp. 149–168, https://doi.org/10.1016/B978-1-78242-087-3.00007-9.
[60] Asma Rostami, Afra Hadjizadeh, Sara Mahshid, Colorimetric determination of dopamine using an electrospun nanofibrous membrane decorated with gold nanoparticles, J. Mater. Sci. 55 (18) (2020) 7969–7980, https://doi.org/10.1007/s10853-020-04547-0.
[61] Yuanfu Zhang, Baoxin Li, Xingling Chen, Simple and sensitive detection of dopamine in the presence of high concentration of ascorbic acid using gold nanoparticles as colorimetric probes, Microchim. Acta. 168 (1-2) (2010) 107–113, https://doi.org/10.1007/s00604-009-0269-5.
[62] Naimeh Mohseni, Morteza Bahram, Highly selective and sensitive determination of dopamine in biological samples via tuning the particle size of label-free gold nanoparticles, Spectrochim. Acta - Part A Mol. Biomol. Spectrosc. 193 (2018) 451–457, https://doi.org/10.1016/j.saa.2017.12.033.
[63] Yanru Bu, Sangwha Lee, Influence of dopamine concentration and surface coverage of Au shell on the optical properties of Au, Ag, and Ag coreAu shell nanoparticles, ACS Appl. Mater. Interf. 4 (8) (2012) 3923–3931, https://doi.org/10.1021/am300750s.
[64] Sergio Dominguez-Medina, Jan Blankenburg, Jana Olson, Christy F. Landes, Stephan Link, Adsorption of a protein monolayer via hydrophobic interactions prevents nanoparticle aggregation under harsh environmental conditions, ACS Sustain. Chem. Eng. 1 (7) (2013) 833–842, https://doi.org/10.1021/sc400042h.
[65] Karuna Giri, Khader Shameer, Michael T. Zimmermann, Sounik Saha, Prabir K. Chakraborty, Anirudh Sharma, Rochelle R. Arvizo, Benjamin J. Madden, Daniel J. Mccormick, Jean-Pierre A. Kocher, Resham Bhattacharya, Priyabrata Mukherjee, Understanding Protein-Nanoparticle Interaction: A New Gateway to Disease Therapeutics, Bioconjug. Chem. 25 (6) (2014) 1078–1090, https://doi.org/10.1021/bc500084f.
[66] E. Ferreira de Macedo, D.M. Ducatti Formaggio, N. Salles Santos, D. Batista Tada, Gold Nanoparticles Used as Protein Scavengers Enhance Surface Plasmon Resonance Signal, Sensors. 17 (2017) 2765, https://doi.org/10.3390/s17122765.
[67] Hanh T.M. Phan, Shannon Bartelt-Hunt, Keith B. Rodenhausen, Mathias Schubert, Jason C. Bartz, Dariush Hinderberger, Investigation of bovine serum albumin (BSA) attachment onto self-assembled monolayers (SAMs) using combinatorial quartz crystal microbalance with dissipation (QCM-D) and spectroscopic ellipsometry (SE), PLoS One. 10 (10) (2015) e0141282, https://doi.org/10.1371/journal.pone.0141282.
[68] Gergo Peter Szekeres, Janina Kneipp, Different binding sites of serum albumins in the protein corona of gold nanoparticles, Analyst. 143 (24) (2018) 6061–6068, https://doi.org/10.1039/C8AN01321G.
[69] G.G.D. La Cruz, P. Rodríguez-Fragoso, J. Reyes-Esparza, A. Rodríguez-López, R. Gómez-Cansino, L. Rodriguez-Fragoso, Interaction of Nanoparticles with Blood Components and Associated Pathophysiological Effects, in: M.P. Sarria, A.C. Gomes (Eds.), Unraveling Saf. Profile Nanoscale Part. Mater. - From Biomed. to Environ. Appl., InTech, 2018: pp. 37–59. https://doi.org/10.5772/intechopen.69386.
[70] Xin Peng, Wei Qi, Renliang Huang, Rongxin Su, Zhimin He, Rizwan H. Khan, Elucidating the influence of gold nanoparticles on the binding of salvianolic acid B and rosmarinic acid to bovine serum albumin, PLoS One. 10 (4) (2015) e0118274, https://doi.org/10.1371/journal.pone.0118274.
[71] S.L. Hirsh, D.R. McKenzie, N.J. Nosworthy, J.A. Denman, O.U. Sezerman, M.M.M. Bilek, The Vroman effect: Competitive protein exchange with dynamic multilayer protein aggregates, Colloids Surf. B Biointerf.. 103 (2013) 395–404, https://doi.org/10.1016/j.colsurfb.2012.10.039.
[72] T. Arentsen, Y. Qian, S. Gkotzis, T. Femenia, T. Wang, K. Udekwu, H. Forssberg, R. Diaz Heijtz, The bacterial peptidoglycan-sensing molecule Pglyrp2 modulates brain development and behavior, Mol. Psychiatry. 22 (2017) 257–266. https://doi.org/10.1038/mp.2016.182.